ACS Catalysis

Research Article

pubs.acs.org/acscatalysis

Hydrogen Adsorption, Dissociation, and Spillover on Ru_{10} Clusters Supported on Anatase TiO_2 and Tetragonal ZrO_2 (101) Surfaces

Hsin-Yi Tiffany Chen, Sergio Tosoni, and Gianfranco Pacchioni*

Dipartimento di Scienza dei Materiali, Università di Milano-Bicocca, via Cozzi 55, 20125 Milano, Italy

Supporting Information

ABSTRACT: The scope of this work is to study at atomistic level the mechanism of hydrogen spillover promoted by metal particles on oxide surfaces. By means of Density Functional Theory calculations with Hubbard correction (DFT+U) we have analyzed the adsorption and dissociation of molecular hydrogen on anatase titania, a-TiO_2 (101), and tetragonal zirconia, t-ZrO_2 (101), surfaces in the presence of a supported Ru_{10} nanocluster. The role of the supported metal particle is essential as it favors the spontaneous dissociation of H_2, a process which does not occur on the bare oxide surface. At low hydrogen coverage, the H atoms prefer to stay on the Ru_{10} particle, charge accumulates on the metal cluster, and reduction of the oxide does not take place. On a hydroxylated surface, the presence of a Ru nanoparticle is expected to promote the reverse effect, i.e. hydrogen reverse spillover from the oxide to the supported metal. It is only at high hydrogen coverage, resulting in the adsorption of several H_2 molecules on the metal cluster, that it becomes thermodynamically favorable to have hydrogen transfer from the metal to the O sites of the oxide surface. In both TiO_2 and ZrO_2 surfaces the migration of an H atom from the Ru cluster to the surface is accompanied by an electron transfer to the empty states of the support with reduction of the oxide surface.

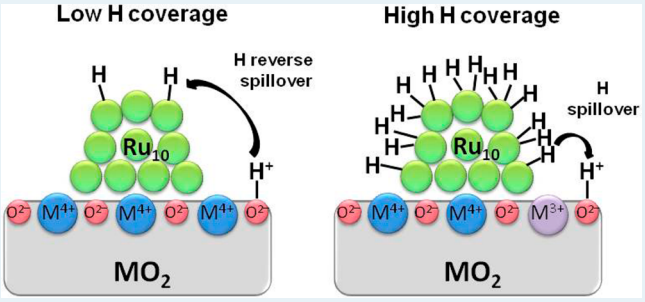

KEYWORDS: *oxide surfaces, metal clusters, hydrogen spillover, DFT, titania, zirconia*

1. INTRODUCTION

Hydrogen plays a fundamental role in chemistry and energy applications. Its interaction with solid surfaces is relevant in hydrogen storage, catalytic hydrogenation of organic substrates, ammonia synthesis, fuel cells, passivation of defects in the microelectronic industry, etc. In heterogeneous catalysis, the adsorption and dissociation of hydrogen on a supported metal particle is a crucial step in many reactions.[1−4] Hydrogen is also used to activate catalysts before their use. For instance, it has been suggested that hydrogen pretreatment results in an increased activity of oxide catalysts like TiO_2 and ZrO_2 for the production of biofuels from cellullosic biomass.[5,6] A key step in bio-oil upgrading is the ketonization of carboxylic acids,[6−8] and it has been shown that the ketonization rate can be increased by adding metal particles, such as Ru, on the surface of the oxide catalyst. This may be related to the formation of coordinatively unsaturated Ti^{3+} and Zr^{3+} sites,[9,10] although a direct confirmation of this mechanism is missing. Calculations performed on Ru and Ni clusters deposited on a-TiO_2 and t-ZrO_2 have excluded the direct reduction of the oxide by metal deposition.[11,12] Oxide reduction can be achieved by hydrogen adsorption in the presence of the deposited metal particles, a phenomenon was observed a long time ago.[13,14] Hoang and Lieske showed that hydrogen pretreatment of ZrO_2 is correlated to catalytic activity at high temperatures in hydrocarbon conversion, presumably due to the presence of catalytically active acid sites.[15]

An important question in this context is the role of the supported metal particle. The status of hydrogen spillover (interphase diffusion of adsorbed hydrogen) has been reviewed,[16] also recently.[17] From the original study of Khoobiar,[18] where it was shown that when Pt/WO_3 is exposed to H_2 the oxide turns blue due to the chemical reduction, many studies have been dedicated to the phenomenon. There is general consensus that the metal particle facilitates the dissociation of the H_2 molecule, thus providing the excess electrons that are needed in order to reduce the surface. This is of key importance in fuel cells.[19] A lot of efforts have been directed at the identification of metals able to efficiently split hydrogen or, even better, of anodes able to oxidize hydrocarbons directly to allow the elimination of internal reforming, $C_mH_{2m+2} + C_nH_{2n+2} \rightarrow C_{m+n}H_{2(m+n)+2} + H_2$. Once atomic hydrogen has been produced from H_2 dissociation, various subsequent steps can be hypothesized. One is that the hydrogen spillover occurs from metal particles (Ru in our case) to the supporting oxide surface (M = Ti or Zr):

Received: May 25, 2015
Revised: July 30, 2015
Published: July 31, 2015

DOI: 10.1021/acscatal.5b01093
ACS Catal. 2015, 5, 5486−5495

$$H_2 + Ru/MO_2 + 2O_{MO_2} \rightarrow 2H/Ru/MO_2 + 2O_{MO_2} \rightarrow Ru/MO_2 + 2OH_{MO_2} \quad (1)$$

In fact, adsorbing metallic particles such as Pt and Rh on ZrO_2 aids the interaction between H and ZrO_2; it has been suggested that H spillover from Pt or Rh to ZrO_2 leads to an increased amount of H on ZrO_2 surfaces.[15,20] The methanol synthesis promoted by Cu/ZrO_2 catalysts has been attributed to the role of Cu in dissociatively adsorbing H_2 and promoting spillover of atomic hydrogen.[21] Zhu reported that by preloading Pt nanoparticles on TiO_2, the hydrogen spillover from Pt to TiO_2 accounts for the increase of hydrogenation capability.[22] Nonetheless, not all TiO_2 supported metal catalysts make H spillover possible. For instance, H spillover was observed for Au/TiO_2[23,24] and Pd/TiO_2 but not for Ni/TiO_2.[25] In general, it is believed that hydrogen spillover does not take place on nonreducible oxides,[16] although the question is still debated for certain cases.

The situation is even more complex if one considers that some reports indicate the spontaneous occurrence of the opposite phenomenon, i.e. hydrogen reverse spillover.[26−29] Here is the hydrogen atom from an OH group of the oxide surface that, in the presence of a supported metal particle, migrates to the supported metal forming multiply hydrogenated metal species. Computational studies revealed that this process is energetically favorable for late transition metals, except for Au.[27,30] Under operative conditions, the occurrence of the direct or reverse hydrogen spillover on reducible oxides depends on the hydrogen partial pressure. By changing this parameter, one changes the hydrogen chemical potential and the direction of the equilibrium.

If direct hydrogen spillover occurs, with migration of hydrogen from the metal particle to the oxide, then the situation is formally analogous to the direct adsorption of H_2 on the oxide surface. When two H atoms are added to the bare MO_2 surface (M = Ti or Zr), they form hydroxyl groups:

$$H_2 + 2O_{MO_2} + 2M^{4+}_{MO_2} \rightarrow 2OH_{MO_2} + 2M^{3+}_{MO_2} \quad (2)$$

The electron associated with atomic H is transferred to a metal cation that changes its oxidation state from M^{4+} to M^{3+} (reduction of the oxide).[31] In the case of hydrogen spillover, however, what remains to be clarified is the nature of the species that diffuses from the metal particle: a neutral H with its valence electron or a proton? In the first case, one electron is moved from the metal cluster to the oxide, with its consequent reduction; in the second case, the electron remains on the metal, which assumes a negative charge, and no direct reduction of the oxide occurs.

Another possibility, at least in theory, is that once the hydrogen has been dissociatively adsorbed on the metal particle, there is a spillover of oxygen from the oxide surface to the metal; the oxygen can react with the hydrogen adsorbed on the metal and form water that then desorbs from the surface:

$$O_{MO_2} + 2H/Ru/MO_2 \rightarrow O/2H/Ru/MO_2 + V_{MO_2} \rightarrow H_2O + Ru/MO_2 + V_{MO_2} \quad (3)$$

This latter mechanism leads to the formation of O vacancies (V_{MO_2}) on the oxide, which is reduced as the consequence of the loss of oxygen and not of the addition of electrons (as in the case of direct H_2 adsorption).

This brief summary is far from being complete and exhaustive, but it illustrates the complexity of the study at the atomistic level of hydrogen adsorption on oxide supported metal nanoparticles. In this work, we try to address the problem and to understand the influence of a Ru nanoparticle on the interaction of H_2 with a-TiO_2 and t-ZrO_2 (101) surfaces and to get an atomistic picture of the adsorption mechanism. We compare, using the same computational setup, the adsorption of a single H atom and the dissociation of one or more H_2 molecules on a Ru_{10} cluster supported on stoichiometric anatase TiO_2 and tetragonal ZrO_2 surfaces. The properties of a Ru_{10} cluster supported on stoichiometric and reduced TiO_2 and ZrO_2 surfaces has been reported previously.[11,12] In this work, we considered as a starting point fully dehydroxylated titania and zirconia surfaces.

The paper is constructed as follows. After some computational details (section 2), in section 3.1 we discuss the adsorption of atomic hydrogen on (a) the bare a-TiO_2 and t-ZrO_2 surfaces, (b) the same surfaces in the presence of a Ru_{10} particle, and (c) directly on the supported metal cluster. In section 3.2 we discuss (a) dissociation of an H_2 molecule on Ru_{10}/TiO_2 and Ru_{10}/ZrO_2, (b) the spillover of one of the two hydrogens from the cluster to the surface, and (c) the effect of the adsorption of several H_2 molecules on the Ru_{10} cluster (saturation coverage). The conclusions are reported in the last section.

2. COMPUTATIONAL METHODS

The calculations are performed using the VASP 5.2 simulation package.[32] The valence electrons, H(1s), O(2s, 2p), Ti(3s, 4s, 3p, 3d), Zr(4s, 5s, 4p, 4d), and Ru(5s, 4p, 4d), are expanded on a set of plane waves with a kinetic cutoff of 400 eV, while the core electrons are treated with the Projector Augmented Wave approach.[33,34] The PBE functional is adopted to calculate the exchange and correlation energy, as formulated in the generalized gradient approximation (GGA) of the density functional theory.[35] The GGA+U approach is applied to the calculation of the electronic structure of TiO_2 and ZrO_2, in order to partially account for the self-interaction error.[36,37] This method partly reduces the underestimation of the electronic band gap and the excessive tendency to delocalize the electron density.[38−40] In this work, we set the Hubbard parameters to U-J = 3 and U-J = 4 eV for Ti and Zr, respectively, which ensures a good qualitative description of structure and electronic properties of Ti and Zr oxides. For example, the relaxed lattice parameters are in reasonable agreement with the experiment (errors on the cell volume <5−6%).[41−43]

There are several polymorphs of TiO_2—anatase, rutile, brookite, and some high pressure phases. Although rutile is the thermodynamically stable bulk phase at all temperatures,[44−46] anatase is the most common phase in catalytic applications.[47−51] The (101) anatase facet is the most stable surface. ZrO_2 can exist in at least five polymorphs.[52,53] Only monoclinic ZrO_2 could stabilize at room temperature; a transition to a tetragonal phase occurs at around 1480 K and transforms into the cubic fluorite phase by increasing the temperature to 2650 K.[54] The monoclinic polymorph has few practical applications due to the brittleness of the structure when cooling from the

DOI: 10.1021/acscatal.5b01093
ACS Catal. 2015, 5, 5486−5495

Table 1. Adsorption energy, E_{ads} (in eV), and Bader Charges, q, of H, Oxides and Ru (in |e|) for an H Atom Adsorbed on a-TiO_2 and t-ZrO_2 (101) Surfaces[a]

system	Figure	E_{ads} (eV)	q(H) |e|	q(MO_2) |e|	q (Ru) |e|	e$^-$ localization
TiO_2−OH	1a	+0.07	+1.00	−1.00		Ti_{5c}
TiO_2−OH	1b	+0.14	+1.00	−1.00		Ti_{6c}
ZrO_2−OH	1c	+0.79	+1.00	−1.00		Zr_{6c}
Ru_{10}(6,4)/TiO_2				−1.28	+1.28	delocalized
Ru_{10}(6,4)/TiO_2−OH	2a	+0.17	+1.00	−2.24	+1.24	Ti_{6c}
Ru_{10}(6,4)/TiO_2−OH	2b	+0.16	+1.00	−2.15	+1.15	delocalized
Ru_{10}(7,3)/ZrO_2				−0.28	+0.28	
Ru_{10}(7,3)/ZrO_2−OH	2c	+0.15	+1.00	−0.91	−0.09	delocalized
Ru_{10}(7,3)/ZrO_2−OH	2d	+0.67	+1.00	−0.93	−0.07	delocalized

[a]The nature of the electron on the oxide, localized or delocalized, is also reported. The associated structures are shown in Figures 1 and 2.

tetragonal phase.[55] The most stable facet of tetragonal ZrO_2, (101), is analogous to the most stable cubic ZrO_2 (111) surface.[56] We have chosen the a-TiO_2 (101) and t-ZrO_2 (101) surfaces for this present study since these are the most stable surfaces of a-TiO_2 and t-ZrO_2, in agreement with previous reports[57−60]

For the relaxation of lattice and internal coordinates of anatase TiO_2 and tetragonal ZrO_2, we used a cutoff of 600 eV and a Γ-centered high-density grid of K-points. Surface properties are studied by means of slab models. Convergence of the electronic structure (density of states) is reached for five-MO_2 layer models (M = Ti or Zr) by fully relaxing both sides of the slabs. For the case of zirconia, also the surface energy is well converged due to the stiffness of the (101) surface.

Then, 3 × 1 and 3 × 2 supercells were used for TiO_2 and ZrO_2, respectively; the sizes of the supercells are 11.5 × 10.5 × 35.0 Å for TiO_2 and 11.0 × 12.9 × 35.0 Å for ZrO_2 (see Figure 2 in ref 11). This corresponds to a composition $Ti_{60}O_{120}$ and $Zr_{60}O_{120}$. The sampling of the reciprocal space is set to the Γ-point, given the relatively large dimension of the supercells. In all cases, at least 10 Å of empty space above the adsorbed species is considered to avoid interactions between the replicas of the slab model.

For all models, we perform structural relaxations of all atoms with convergence criteria of 10^{-5} eV and 10^{-2} eV/Å for the electronic and ionic loops, respectively. Atomic charges have been determined according to the Bader partition method.[61]

3. RESULTS AND DISCUSSION

3.1. H Atom Adsorption. *H Adsorption on TiO_2 and ZrO_2.* In general, irreducible metal oxides, like MgO, induce the heterolytic splitting of H_2 with formation of M^{n+}−H^- and $O^{2-}H^+$ species;[62,63] on the contrary, on reducible metal oxides such as TiO_2 or ZrO_2, homolytic dissociation occurs with the formation of surface hydroxyls.[64−71] In this case, two electrons are transferred from the H_2 molecule to the oxide, with direct reduction of the metal cations from M^{n+} to $M^{(n-1)+}$, eq 2.

Assuming that H_2 dissociation has already taken place (see below), we adsorbed the H atom on a 2-fold-coordinated O_{2c} site of a-TiO_2 and a 3-fold-coordinated O_{3c} site of t-ZrO_2 (101) surfaces; the optimal O−H bond length is 0.97 Å for both oxides. Of course, the H coverage affects the adsorption energy,[69] but here we consider an isolated H atom (with the supercells used, the coverage is of 1/36 monolayer, ML). The H adsorption energy is defined with respect to gas-phase H_2:

$$E_{ads} = E(H/MO_2) - E(MO_2) - 1/2E(H_2) \quad (4)$$

E_{ads}, see Table 1, is positive for both oxides, indicating an endothermic reaction. In both a-TiO_2 and t-ZrO_2, one electron is transferred to Ti 3d and Zr 4d empty states with the formation of an adsorbed proton, H^+, and Ti^{3+} and Zr^{3+} ions, respectively, as shown by the spin density plots of Figure 1. The

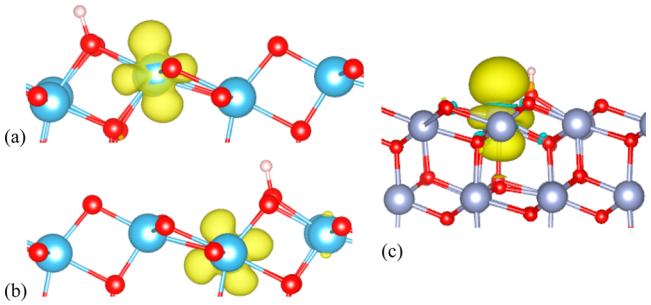

Figure 1. Spin density plot of a H atom adsorbed on a O site of (a and b) a-TiO_2 and (c) t-ZrO_2 (101) surfaces. The excess electron is trapped on (a) Ti_{5c}, (b) Ti_{6c}, and (c) Zr_{6c}. See also Table 1. Blue, Ti; violet, Zr; red, O; white, H. The isosurface corresponds to 0.005|e|/Å^3.

presence of an unpaired electron trapped on the oxides is shown also by the analysis of the spin population and of the Bader charge which shows an overall negative charge of −1.0|e| on the oxide after H adsorption, Table 1.

It should be mentioned at this point that the identification of Ti^{3+} ($3d^1$) and Zr^{3+} ($4d^1$) sites is a complex issue. It depends on the details of the computational approach used (larger U parameters result in more localized solutions) and on the polaronic distortion that accompanies the formation of reduced M^{3+} centers.[72] Sometimes, to obtain a localized solution, one has to manually distort the lattice in order to favor the formation of the polaron during the geometry optimization. Of course, several possible solutions exist.[72] These solutions are relatively close in energy, and the barriers needed to induce electron mobility are relatively low. In both rutile and anatase TiO_2, they have been estimated and are on the order of 0.3 eV.[73] This means that at the temperatures relevant for the catalytic processes, the trapped electrons will rapidly hop from one site to another, resulting in considerable electron mobility. For this reason, a detailed discussion of the nature of the reduced M^{3+} sites, useful to show the occurrence of a reduction of the oxide, is not relevant for the modeling of the catalytic processes following reduction by hydrogen adsorption.

On a-TiO_2, we have been able to obtain two different solutions, one with the electron trapped on a Ti_{5c} ion and one where the electron goes to a Ti_{6c} ion. The corresponding

DOI: 10.1021/acscatal.5b01093
ACS Catal. 2015, 5, 5486−5495

adsorption energies are +0.07 and +0.14 eV, respectively, Table 1. This means that H_2 is not expected to spontaneously dissociate on the regular surface of a-TiO_2, in agreement with previous work.[70,71,74]

The reaction is even more endothermic on t-ZrO_2 where E_{ads} is +0.79 eV, Table 1. This reflects the fact that in ZrO_2 the bottom of the conduction band is much higher than in TiO_2, by 1.5 eV according to our DFT calculations (see Figure 1 in ref 11), and that it is more unfavorable to transfer one electron from the H atom to the Zr 4d empty states. Notice that on ZrO_2, a less reducible oxide than TiO_2, previous theoretical calculations have reported the possible occurrence of a heterolytic splitting of H_2 with formation of a hydride, Zr−H, and an OH groups.[75] Of course, this process does not lead to a reduction of the zirconia.

These results show that H_2 dissociation with formation of protons adsorbed on O ions and electrons trapped at cation sites does not occur on the regular surfaces of a-TiO_2 and t-ZrO_2. The presence of deposited metal particles is thus essential for the process, as will be discussed in the next section.

H Adsorption on Surface O of Ru_{10}/TiO_2 and Ru_{10}/ZrO_2. Here, we consider the properties of atomic H adsorbed on the surface of a-TiO_2 and t-ZrO_2 in the presence of a Ru_{10} nanoparticle. The question we want to address is whether the supported metal cluster has an effect on the adsorption properties and electronic structure of the oxide or not. To this end, we considered H adsorption on the same O sites of the two oxide supports with a neighboring Ru_{10} cluster, Table 1 and Figure 2. The Ru_{10} cluster is at 2.7 and 4.6 Å, respectively, from the OH group (shortest Ru−H distance) for the case of TiO_2 and ZrO_2. Following our previous work,[11] two different isomers of Ru_{10} have been considered, one with seven atoms at the interface and three on the top layer, $Ru_{10}(7,3)$, and one with six interface Ru atoms and four in the top layer, $Ru_{10}(6,4)$. $Ru_{10}(6,4)$ is more stable on TiO_2 while $Ru_{10}(7,3)$ is more stable on ZrO_2, so the analysis is performed with respect to these two isomers (but we checked that the results do not change if the other isomer is considered). The adsorption energy is defined with respect to each isomer:

$$E_{ads} = E(H/Ru_{10}(n, m)/MO_2) - E(Ru_{10}(n, m)/MO_2) - 1/2E(H_2) \quad (5)$$

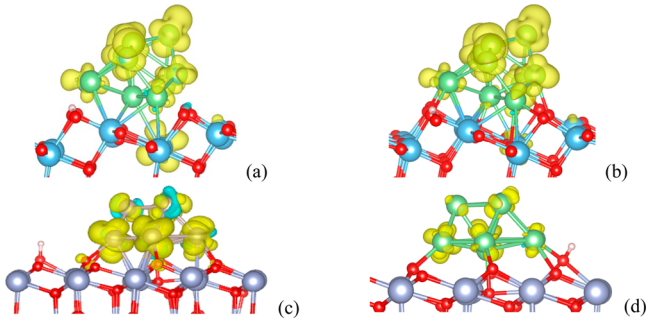

Figure 2. Spin density (in yellow) of a hydrogen atom adsorbed on (a) O_{2c} of Ru_{10}/TiO_2 with one electron localized on Ti_{6c}, (b) O_{2c} of Ru_{10}/TiO_2 with one electron delocalized, (c) O_{3c} of Ru_{10}/ZrO_2, and (d) interface O_{3c} of Ru_{10}/ZrO_2. See also Table 1. Blue, Ti; violet, Zr; red, O; green, Ru; white, H. The isosurface corresponds to 0.005|e|/Å^3.

For TiO_2, we do not observe any significant variation in the properties with respect to the case where H has been adsorbed on the clean surface (no supported Ru), Table 1. The adsorption energy remains slightly positive, 0.16 eV, and the electronic charge is transferred to the oxide. We have been able to obtain two solutions, one where the spin is entirely localized on a Ti ion (Ti^{3+}), Figure 2a, and one where the charge is delocalized, Figure 2b. The difference in energy between the two solutions is negligible, Table 1, showing that the localization does not lead to an important stabilization. In both cases, the Bader charge indicates an accumulation of negative charge in the oxide, $\Delta q \approx -1.0|e|$, which is a sign of the occurrence of a chemical reduction. From these results, we can conclude that there is no beneficial long-range effect of the Ru_{10} nanoparticle on the H adsorption on TiO_2.

The situation is rather different when we consider the same process on ZrO_2. In this case, in fact, the formation of an OH group in the presence of Ru_{10}, Figure 2c, has an adsorption energy, +0.15 eV, that is still endothermic, but 0.64 eV more favorable than on the bare surface, see Table 1. One electron is transferred to the oxide, as shown by the Bader charge, $\Delta q \approx -1.0|e|$. However, no spin localization on a Zr ion is found, despite several attempts. Rather, the charge accumulates on a few Zr ions below the Ru_{10} cluster, which also becomes slightly negatively charged, Table 1. This seems to suggest a role of the supported metal particle in inducing accumulation of the extra electron at the metal/oxide interface. Notice that if the hydrogen is adsorbed on an O atom at the metal−oxide interface, Figure 2d, the adsorption energy is +0.65 eV, indicating that the proton prefers to be far from the metal particle.

H Adsorption on Ru Atoms of Ru_{10}/TiO_2 and Ru_{10}/ZrO_2. The results on the adsorption of H on O_{nc} sites of the titania

Table 2. Adsorption Energy, E_{ads} (eV), Ru−H Bond Lengths (Å), and Bader Charges, q, of H, Oxides, and Ru (in |e|) for a Single Hydrogen Atom Adsorbed on Ru_{10}/TiO_2 and Ru_{10}/ZrO_2 (101) Surfaces[a]

system	Figure	adsorption site[b]	E_{ads} (eV)	r(RuH) (Å)	q(H) |e|	q(MO_2) |e|	q(Ru) |e|
H/Ru_{10}(6,4)/TiO_2	3a	Ru_{top}	−0.65	1.66	−0.26	−1.22	+1.48
H/Ru_{10}(6,4)/TiO_2	3b	Ru_{bridge}	−0.50	1.79, 1.82	−0.26	−1.28	+1.53
H/Ru_{10}(7,3)/TiO_2		Ru_{top}	−0.78	1.64	−0.23	−1.15	+1.38
H/Ru_{10}(7,3)/TiO_2		Ru_{bridge}	−0.45	1.74, 2.04	−0.27	−1.19	+1.46
H/Ru_{10}(7,3)/TiO_2		interface	+0.09	1.80, 1.82	−0.21	−1.18	+1.39
H/Ru_{10}(7,3)/ZrO_2	3c	Ru_{top}	−0.48	1.65	−0.26	−0.25	+0.50
H/Ru_{10}(7,3)/ZrO_2	3d	Ru_{bridge}	−0.35	1.79, 1.80	−0.24	−0.24	+0.47
H/Ru_{10}(7,3)/ZrO_2		Ru_{hollow}	−0.17	1.85, 1.88	−0.16	−0.27	+0.43

[a]The associated structures are shown in Figure 3. [b]Several configurations of H adsorption on a Ru hollow site were computed; however, the H moves spontaneously to the bridge site.

DOI: 10.1021/acscatal.5b01093
ACS Catal. 2015, 5, 5486−5495

and zirconia surfaces has shown that even the presence of an adsorbed Ru nanoparticle does not lead to an exothermic process, Table 1. Now, we consider the direct adsorption of H on the Ru cluster. We have placed the H atom on several positions of Ru_{10} and at the Ru_{10}/MO_2 interface (see also Figure S1 in Supporting Information). For brevity, we will discuss only the most stable structures, Table 2.

The first observation is that when H is adsorbed on Ru_{10}, E_{ads} is always negative, indicating a favorable process. The binding of H to Ru can result in an energy gain of about 0.6 eV with respect to the free H_2 molecule, Table 2 and Figure 3a. This

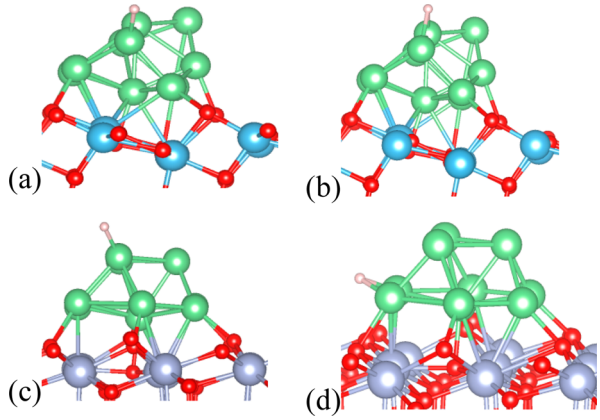

Figure 3. Structures of a hydrogen atom adsorption on different sites of Ru_{10}/TiO_2 and Ru_{10}/ZrO_2 (101) surfaces. (a) Ru_{10}/TiO_2, H on top of Ru; (b) Ru_{10}/TiO_2, H on Ru bridge site; (c) Ru_{10}/ZrO_2, H on top of Ru; (d) Ru_{10}/ZrO_2, H on Ru bridge site. See also Table 2. Blue, Ti; violet, Zr; red, O; green, Ru; white, H.

result clearly indicates the net preference for H to bind to the metal particle with respect to the oxide surface. In general, the binding of H on top of Ru is preferred compared to the bridge sites, see e.g. Figure 3a and b. The Ru−H bond length is around 1.7 Å. When the H atom is placed on Ru but near the metal/titania interface, it induces a geometrical rearrangement with one O_{2c} atom that protrudes outward from the surface (not shown). The adsorption energy, however, is positive. This suggests, together with the result reported above for ZrO_2, that the interface is not a favorable region for H adsorption.

Turning to Ru_{10}/ZrO_2 structures (Figure 3c and d), the H adsorption energies range from −0.48 to −0.17 eV, Table 2. Thus, the adsorption energy on TiO_2 (in absolute value) is about 0.2 eV larger than on ZrO_2, suggesting that the support has an effect on the adsorption properties of the metal particle and that hydrogen adsorption is preferred on Ru_{10}/TiO_2 compared to Ru_{10}/ZrO_2. For the case of Ru_{10}-ZrO_2, we performed some tests on the adsorption of H on a gas-phase $Ru_{10}(7,3)$ particle. On an on-top site of $Ru_{10}(7,3)$, the adsorption energy is −0.73 eV (fully relaxed cluster); this reduces to −0.61 eV if the Ru atoms are frozen into the positions they assume on t-ZrO_2. We also computed by an energy decomposition the relaxation energy induced by H adsorption. This turns out to be negligible in the case of Ru_{10}/TiO_2 (<0.01 eV), while it is larger (0.12 eV) for Ru_{10}/ZrO_2. The lower binding energy of H to Ru_{10}/ZrO_2 is therefore due to the cost of deforming the Ru_{10} cluster when an H atom is added.

We consider now the charge distribution. The Bader charges clearly indicate that moving the H atom from the surface (OH group) to the particle (Ru−H bond) results in the displacement of electronic charge from the oxide to the $Ru_{10}H$ complex. Since the H atom adsorbed on a metal particle assumes a hydride character (on Ru_{10}, the H atom is negatively charged, see Table 2), it has the property to "oxidize" the metal particle (as shown by the positive charge on Ru_{10}, Table 2). This is an important result which shows that the displacement of a proton from an O_{nc} site of the oxide to a Ru atom of the particle (or viceversa) is accompanied by a corresponding electron transfer.

3.2. Adsorption of H_2 Molecule. *Dissociative Adsorption on Ru_{10}/TiO_2 and Ru_{10}/ZrO_2.* So far, we have considered the adsorption of a single H atom on either the oxide surface or on the supported Ru cluster. In doing this, we have assumed that dissociation has occurred at some stage. In this section, we consider the dissociative adsorption of H_2 on Ru_{10}/TiO_2 and Ru_{10}/ZrO_2. The first important result is that by placing the hydrogen molecule close to the metal cluster we observe a spontaneous dissociation on both systems, indicating a nonactivated process. Also, here we considered two different Ru_{10} isomers, and the adsorption energies per H atom are obtained according to the following equation:

$$E_{ads} = [E(xH_2/Ru_{10}(n, m)/MO_2) - E(Ru_{10}(n, m)/MO_2) - xE(H_2)]/2x \quad (x = 1 - 15) \qquad (6)$$

The most stable configurations on Ru_{10}/TiO_2 exhibit adsorption energies per H atom around −0.55 to −0.48 eV, see Table 3 and Figure 4a and b. With respect to a single H atom on the same $Ru_{10}(6,4)/TiO_2$ cluster (E_{ads} −0.65 eV, Table 2), there is a modest reduction of the adsorption energy, an effect that will be relevant for the following discussion.

On Ru_{10}/ZrO_2, the most stable configurations show an adsorption energy per atom of −0.44 eV, Table 3 and Figure 4c

Table 3. Adsorption Energy per H Atom, $E_{ads/H}$, (in eV) and Bader Charges, q, of Ru, H, and Oxides (in |e|) for a H_2 Molecule Dissociatively Adsorbed on Ru_{10}/a-TiO_2 and Ru_{10}/t-ZrO_2 (101) Surfaces[a]

system	Figure	adsorption site	$E_{ads/H}$ (eV)	q(Ru), |e|	q(H), |e|	q(MO_2), |e|
$2H/Ru_{10}(6,4)/TiO_2$	4a	Ru_{top} + Ru_{top}	−0.55	+1.77	−0.41	−1.36
$2H/Ru_{10}(6,4)/TiO_2$	4b	Ru_{top} + Ru_{bridge}	−0.48	+1.83	−0.44	−1.39
$1H/Ru_{10}(6,4)/TiO_2$−OH[b]		Ru_{top} + O_{2c}	−0.26	+1.37	+0.73	−2.10
$1H/Ru_{10}(6,4)/TiO_2$−OH[c]		Ru_{top} + O_{2c}	−0.22	+1.44	+0.73	−2.17
$2H/Ru_{10}(7,3)/ZrO_2$	4c	Ru_{top} + Ru_{bridge}	−0.44	+0.68	−0.49	−0.19
$2H/Ru_{10}(7,3)/ZrO_2$	4d	Ru_{top} + Ru_{top}	−0.44	+0.70	−0.46	−0.23
$2H/Ru_{10}(7,3)/ZrO_2$		Ru_{bridge} + Ru_{bridge}	−0.26	+0.85	−0.54	−0.30
$1H/Ru_{10}(7,3)/ZrO_2$−OH		Ru_{top} + O_{3c}	−0.06	+0.15	+0.74	−0.90

[a]The associated structures are shown in Figure 4. [b]One excess electron delocalizes on Ti atoms. [c]One excess electron localizes on one Ti_{6c} atom

DOI: 10.1021/acscatal.5b01093
ACS Catal. 2015, 5, 5486−5495

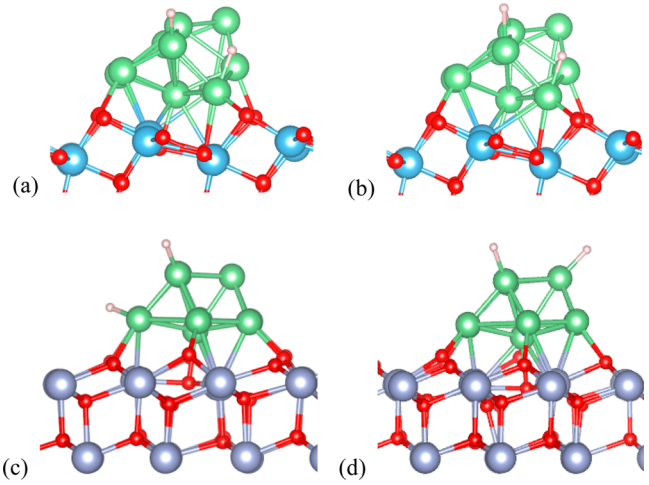

Figure 4. Structures of a H_2 molecule dissociatively adsorbed on different active sites of Ru_{10}/TiO_2 (a and b) and Ru_{10}/ZrO_2 (101) surfaces (c and d). See also Table 3. Blue, Ti; violet, Zr; red, O; green, Ru; white, H.

and d. Here, the reduction of the average adsorption energy compared to the case of a single H adsorption, $E_{ads} = -0.48$ eV, is negligible.

From an electronic point of view, the addition of two H atoms to the cluster instead of one does not change the general picture. In particular, the H atoms remain negatively charged and oxidize the metal particle, Table 3, and most important, there is no sign of an electron transfer from the metal cluster to the oxide by adsorption of a pair of H atoms. To summarize, we can conclude that the role of the supported metal nanoparticle is essentially to adsorb and split the H_2 molecule with a nonactivated and thermodynamically favorable process.

Hydrogen Spillover on Ru_{10}/TiO_2 and Ru_{10}/ZrO_2. In this section, we consider a case where, after an H_2 molecule has been dissociatively adsorbed on the Ru_{10} supported cluster, one H atom remains on the metal cluster (top of a Ru atom) while the second one is displaced to a surface O_{2c} (TiO_2) or O_{3c} (ZrO_2) atom. This is the simplest model of H spillover, and the comparison with the previous results can provide indications about (1) the energetic of the process and (2) the electronic changes accompanying the spillover of hydrogen to the surface.

In both TiO_2 and ZrO_2, the system with two H atoms adsorbed on the metal cluster is considerably more stable compared to the case where one H has migrated to the oxide (compare $2H/Ru_{10}/MO_2$ with $1H/Ru_{10}/MO_2$–OH in Table 3). In particular, $E_{ads/H}$ goes from −0.55 eV to −0.26 eV on TiO_2 and from −0.44 eV to −0.06 eV on ZrO_2, reflecting the unfavorable binding to O compared to Ru. The displacement of the H atom from Ru_{10} to the TiO_2 or ZrO_2 surfaces is accompanied by an electron transfer and by the consequent reduction of the surface. On TiO_2, by displacing the H atom, the charge on the oxide goes from −1.36 |e| to −2.10|e| with a $\Delta q = -0.74|e|$; on ZrO_2 the charge goes from −0.19|e| to −0.90 |e| with $\Delta q = -0.71|e|$, Table 3. This confirms that the diffusing species is an H atom and not a proton (in this latter case, the extra electron would remain on the metal cluster). For TiO_2, we also observe that the extra electron localizes on a Ti_{6c} atom near the OH group; the delocalized solution is very close in energy (Table 3).

Multiple Adsorption of H_2 Molecules on Ru_{10}/TiO_2 and Ru_{10}/ZrO_2. In the previous sections, we have shown that direct spontaneous spillover of hydrogen from the metal to the oxide does not occur, at least for low hydrogen coverage where the relative energy state for hydrogen on the metal is lower than for hydrogen on the oxide. However, the energy states available for hydrogen will depend on the degree of saturation (or substrate coverage), which, in turn, depends on the hydrogen partial pressure.

At high hydrogen exposure, the supported particle can adsorb hydrogen until saturation is reached. At that point, hydrogen will spill over to the oxide. Metal particles can adsorb large quantities of hydrogen before reaching saturation. Calculations performed on a gas-phase Pt_6 cluster have shown that the average dissociative chemisorption energy of H_2 decreases regularly by adding more molecules to the cluster, but after the addition of 13 H_2 molecules the cluster can still adsorb hydrogen and is not saturated.[76] In a similar recent study, it was shown that a Pd_4 cluster can adsorb up to nine H_2 molecules. When supported on a graphitic support, the spillover from Pd_4 to the support is thermodynamically favorable after the catalyst has adsorbed 12 H atoms, i.e., three H atoms per metal atom in the cluster.[77] Assuming a similar hydrogen adsorption capability of Ru as for Pd, we can expect that H spillover can occur on our Ru_{10}/TiO_2 and Ru_{10}/ZrO_2 systems only after about 30 hydrogen atoms have been adsorbed on the catalyst. Notice however that for other metals, e.g. Pt, it has been suggested that a Pt/H ratio of 1:4 is necessary to reach saturation.[76]

We have tested the adsorption capability of Ru_{10}/TiO_2 by adding an increasing number of H atoms, Table 4 and Figure 5. Of course, by adding increasing amounts of hydrogen, the structure of the cluster changes and a large number of isomers exists in principle. This has been shown in a careful study of Pt clusters supported on γ-Al_2O_3. Using a combination of X-ray

Table 4. Adsorption Energy, E_{ads}, (in eV); Adsorption Energy per H Atom, $E_{ads/H}$, (in eV); Bader Charge, q, of Ru, H, and Oxides (in |e|) for Multiple H Atom Adsorption on Ru_{10}/a-TiO_2 and Ru_{10}/t-ZrO_2 (101) Surfaces

system	E_{ads} (eV)	$E_{ads/H}$ (eV)	q(Ru), |e|	q(H), |e|	q(MO_2), |e|
$12H/Ru_{10}(6,4)/TiO_2$	−4.40	−0.37	+3.09	−1.76	−1.33
$11H/Ru_{10}(6,4)/TiO_2$–OH	−3.86	−0.32	+2.82	−0.70	−2.12
$16H/Ru_{10}(5,5)/TiO_2$	−6.19	−0.39	+3.13	−1.95	−1.18
$15H/Ru_{10}(5,5)/TiO_2$–OH	−5.79	−0.36	+2.99	−1.02	−1.97
$24H/Ru_{10}(6,4)/TiO_2$	−7.27	−0.30	+3.26	−2.52	−0.74
$23H/Ru_{10}(6,4)/TiO_2$–OH	−7.14	−0.30	+3.16	−1.52	−1.64
$30H/Ru_{10}(5,5)/TiO_2$	−8.72	−0.29	+3.42	−2.47	−0.95
$29H/Ru_{10}(5,5)/TiO_2$–OH	−8.95	−0.30	+3.54	−2.12	−1.42
$12H/Ru_{10}(7,3)/ZrO_2$	−5.23	−0.44	+2.88	−2.97	+0.10
$11H/Ru_{10}(7,3)/ZrO_2$–OH	−3.87	−0.32	+2.06	−1.48	−0.58
$16H/Ru_{10}(7,3)/ZrO_2$	−5.99	−0.37	+2.31	−2.28	−0.03
$15H/Ru_{10}(7,3)/ZrO_2$–OH	−5.20	−0.33	+2.20	−1.56	−0.65
$24H/Ru_{10}(7,3)/ZrO_2$	−9.10	−0.38	+3.14	−3.23	+0.09
$23H/Ru_{10}(7,3)/ZrO_2$–OH	−9.38	−0.39	+2.87	−2.34	−0.53
$30H/Ru_{10}(7,3)/ZrO_2$	−9.38	−0.31	+3.23	−3.49	+0.26
$29H/Ru_{10}(7,3)/ZrO_2$–OH	−9.49	−0.32	+3.02	−2.58	−0.44

DOI: 10.1021/acscatal.5b01093
ACS Catal. 2015, 5, 5486−5495

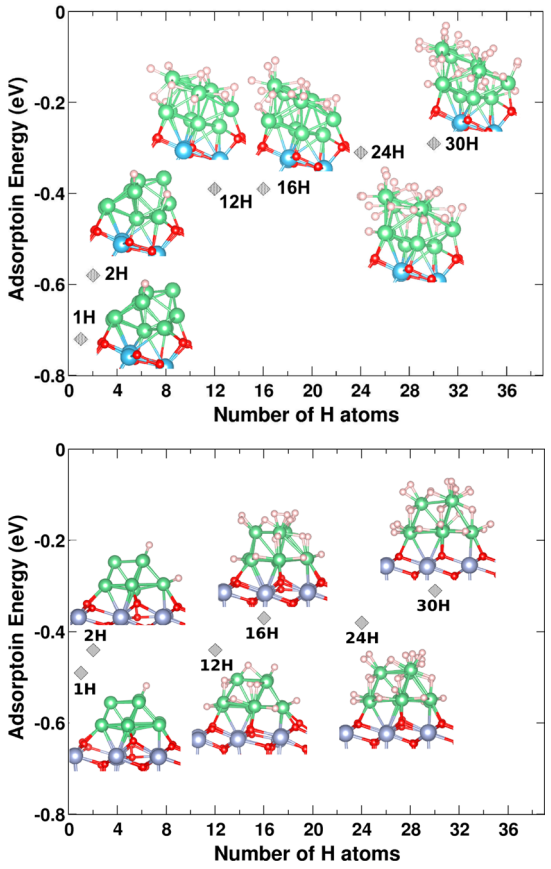

Figure 5. Calculated average adsorption energy per H atom against the number of H atoms on Ru_{10}/TiO_2 (top) and Ru_{10}/ZrO_2 (bottom). The structure of the hydrogenated clusters is shown in the insets.

adsorption near edge structure (XANES) and DFT molecular dynamics simulations, it has been possible to show that the Pt cluster undergoes substantial reconstruction by increasing the hydrogen coverage.[78,79] Here, while we considered a few possible structures, we did not attempt a complete search of the optimal structure. The various isomers have been constructed following some guiding principles. Hydrogen has been preferentially added on the second layer of the Ru_{10} cluster, as these sites appeared to be preferred with respect to adsorption at interface Ru atoms. Once the top Ru layer has been saturated, hydrogen has been added also to the interface Ru atoms. Formation of hydride structures, with H atoms inside the Ru_{10} cluster, has also been considered for zirconia but resulted in less stable configurations or in the spontaneous displacement of hydrogen toward the surface of the cluster.

In general, we found that the general trends are similar for different Ru structures, and in particular, the average hydrogen adsorption energy is similar for different Ru_{10} isomers.

We start from a single H atom. As discussed above, H is bound to $Ru_{10}(6,4)/TiO_2$ with E_{ads} = −0.65 eV, Table 2; if H is displaced to an O atom of the oxide surface, the system becomes unbound (with respect to H_2) by +0.07 eV, Table 1. The adsorption of two H atoms, one on the cluster and one on the oxide, leads to a reduced $E_{ads/H}$ = −0.55 eV/atom, Table 3, i.e. 0.1 eV smaller than for the case of single H adsorption. Next, we added 12 H atoms. The total energy release is much lower than in the previous cases; $E_{ads/H}$ becomes −0.37 eV/atom, about 0.2 eV/atom smaller than for 2 H atoms adsorption, Table 4. Once 12 H atoms have been added, the displacement of one H atom from Ru to the oxide is still unfavorable by 0.54 eV, Table 4. With respect to the displacement of a single H atom from the cluster to the oxide (see Table 1 and 2), the thermodynamic energy cost is decreased by 0.28 eV. With 16 H atoms, the average adsorption energy when the Ru particle is involved is 0.39 eV/atom; the displacement of one H to the oxide has a cost of 0.4 eV, Table 4. Next, we have considered the addition of 24 H atoms to Ru_{10}/TiO_2. Also, in this case, we have considered different Ru_{10} structures, but the final value of $E_{ads/H}$ is very similar, about −0.3 eV/atom, Table 4. Thus, there is a slow but not monotone decrease in adsorption energy as the amount of hydrogen increases, Figure 5. Also in this case, we have considered the displacement of an H atom from the Ru_{10} cluster to the TiO_2 surface, and we found that the energy cost for the spillover has reduced to 0.13 eV only, Table 4. Thus, even after the addition of 24 H atoms on Ru_{10}, direct spillover is not spontaneous. The turnover occurs when we adsorb 30 H atoms. $E_{ads/H}$ is still negative, −0.29 eV/atom. However, the structure where all the H atoms are adsorbed on the metal particle is 0.23 eV less stable than that where an OH group has been formed, see Table 4 and Figure 5. These results clearly show that H spillover becomes thermodynamically favorable only at high H loading, when around 3 H atoms adsorbed for then Ru atom in the cluster.

We also tried to estimate the barrier for diffusion of one H atom from the Ru_{10} cluster to the TiO_2 surface. To this end, we have considered one H atom bound to the bottom layer of Ru_{10} in the $30H/Ru_{10}/TiO_2$ structure. Using the climbing-image Nudged elastic band (NEB) method,[80] we have calculated the barrier for diffusion of this atom from the supported metal cluster to the TiO_2 surface, where it forms a surface OH group. The final structure is 0.23 eV more stable than the initial one (see above), and the barrier is 0.4 eV (see Figure S2 in the Supporting Information). This relatively low barrier is consistent with the occurrence of hydrogen spillover at the operating temperatures of real catalytic processes.

We notice that by increasing the hydrogen coverage, not all the H_2 molecules are fully dissociated. Taking 1.2 Å as a criterion for complete H−H dissociation, we found that for the highest coverage about one-half of the adsorbed molecules are still in an activated molecular adsorption form (see Table S1 in the Supporting Information).

In terms of electronic properties, we notice that the subsequent addition of H on the Ru_{10} cluster on TiO_2 has two effects: (1) the H atoms bound to Ru have hydride character and lead to the partial oxidation of the metal particle; (2) the cluster magnetic moment is progressively quenched by the addition of H until, for the 30 H atoms case, a zero magnetic moment is reached.

At low loading of hydrogen, $Ru_{10}(7,3)/ZrO_2$ displays a rather different behavior compared to what was reported for titania. In particular, we observe almost no decrease in adsorption energy passing from to 2 to 12 H. Also at loadings of 16 and 24 H, the adsorption energy per H atom remains close to −0.4 eV, Table 4. Saturation effects start to be visible at 30 H atoms, where the adsorption energy eventually decreases to −0.31 eV. A further decrease is observed for 40 H (−0.29 eV) and 45 H (−0.23 eV). The spillover cost remarkably decreases from 1.4 eV at 12 H to 0.8 eV at 16 H and becomes thermodynamically favorable at 24 H coverage, Table 4. Also in this case, the analysis of the Bader charges reveals that there is no relevant charge transfer to the oxide as long as all H atoms remain on the metal particle. H

DOI: 10.1021/acscatal.5b01093
ACS Catal. 2015, 5, 5486−5495

spillover, on the contrary, always implies a remarkable electron transfer to the surface.

The metal particle on zirconia is remarkably rigid compared to what is observed on titania: no isomerization nor major distortion is observed up to H_{30}. This may be a key to understanding the different behavior of Ru_{10} on the two considered supports. We also notice that H atoms prefer in general to stay adsorbed on the surface of the cluster, and only for high H coverage (>30 H atoms) do some atoms go inside the cluster and form a kind of hydride species. Differently from titania, on Ru_{10}/ZrO_2 even at high coverage, almost all the H_2 molecules are fully dissociated. For the highest loading, we find at most two to three molecules in molecular adsorption form (see Table S1 in the Supporting Information).

The results reported above show that only at high partial pressures hydrogen can spill over from the cluster and diffuse to the oxide surface. The results also show that the migration of H is accompanied by the reduction of the oxide. The evidence of the reduction comes from the analysis of the Bader charges (the negative charge on the oxide increases as a consequence of the spillover); in some cases, we have also been able to observe the formation of Ti^{3+} or Zr^{3+} species. Also in this case, at high hydrogen coverage, we notice that the H displacement is accompanied by a regular increase of the negative charge on the oxide, an effect which is basically independent of the total hydrogen coverage. In particular, the negative charge on the Ru_{10}/TiO_2 clusters is $\Delta q = -0.79|e|$ (12 H atoms), $\Delta q = -0.79|e|$ (16 H atoms), $\Delta q = -0.90|e|$ (24 H atoms), and $\Delta q = -0.47|e|$ (3 0H atoms), Table 4. A similar trend is found for ZrO_2, see Table 4.

One should mention at this point that we considered in our models fully dehydroxylated titania and zirconia surfaces. Under working catalytic conditions, the surface can become hydroxylated and the process of hydrogen spillover can be affected by the level of hydroxylation of the surface.[81,82]

In principle, another reduction mechanism is also possible. At high hydrogen partial pressure, when the metal particle is covered by hydrogen, O atoms from the surface can diffuse to the metal (O reverse spillover). Oxygen can react with hydrogen and form water that can then leave the surface. The process results in the removal of O from the oxide and in the release of water, facilitated by the presence of hydrogen. This provides another channel for the chemical reduction of the oxide indirectly related to the addition of hydrogen. We have considered this mechanism for two systems: 12 $H/Ru_{10}/TiO_2$ and 30 $H/Ru_{10}/TiO_2$. In both cases, the desorption of a H_2O molecule with formation of an O vacancy on the surface of the oxide is an uphill process, unfavorable by 1.9 eV. Even considering entropic effects, it is unlikely that the process will take place. Since the O vacancy formation energy is higher in ZrO_2 than in TiO_2, this conclusion applies to zirconia as well.

4. CONCLUSIONS

In this study, we have considered the energetics of adsorption, dissociation, and migration of hydrogen on models of Ru nanoparticles supported on titania and zirconia surfaces. We have found, in agreement with previous studies, that neither TiO_2 nor ZrO_2 surfaces are able to split H_2. On titania, the cost is rather small, 0.07 eV, while on zirconia it is considerably higher, 0.79 eV. This is due to the fact that the formation of a hydroxyl group is accompanied by a transfer of the H valence electron to a Ti 3d or Zr 4d empty state at the bottom of the oxide conduction band. Since the conduction band in ZrO_2 is considerably higher than on TiO_2, the process is energetically less favorable. The presence of a Ru nanoparticle has no effect on the H adsorption properties of TiO_2 (both the adsorption energy and charge distribution are essentially unaffected) while it has some effect on ZrO_2. Here, in fact, once the OH group is formed, the excess charge goes preferentially at the metal/oxide interface, lowering the cost for the dissociative adsorption.

Adsorption of H on the O sites of the surfaces is not competitive with adsorption on the metal nanoparticle. H adsorbs on Ru_{10}, preferentially on top of Ru atoms, forming a strong Ru−H bond with hydride character. The interaction is such that spontaneous nonactivated dissociation of an H_2 molecule occurs on the Ru cluster which has the effect of splitting hydrogen and to bind a large amount of H atoms.

Therefore, the adsorption of an H atom on the surface of TiO_2 or ZrO_2 is endothermic if one takes as a reference the H_2 molecule. It is exothermic if it is referred to an H atom. The role of the Ru_{10} cluster is to split the H_2 molecule in a barrierless process and to generate isolated H atoms that can diffuse to the oxide surface once saturation coverage on the cluster has been reached.

Direct spillover from the metal particle to the oxide surface is not favorable at low hydrogen coverage. For the hypothetical case of the dissociation of a single H_2 molecule on the Ru cluster, with one H atom that remains bound to the metal and the other one that diffuses to the oxide, the cost is about 0.3−0.4 eV, Table 3. This cost, however, decreases gradually as more hydrogen is adsorbed on the metal cluster. At a coverage of 30 H atoms on Ru_{10}/TiO_2, i.e., a Ru/H ratio of 1:3, it becomes thermodynamically favorable to move one H from the metal to the oxide. On zirconia, the effects appear already for a coverage of 24 H atoms. In this study, we did not consider in detail the kinetic aspects of the problem. However, we estimated the cost of the diffusion of the H atom from the metal particle to the TiO_2 surface, and we found a process where this barrier is 0.4 eV. Since many other paths are possible, this value represents an overestimate. Previous detailed studies on hydrogen diffusion on the anatase TiO_2 (101) surface have shown that hydrogen preferentially diffuses into the bulk compared to the surface, and that the smallest barrier for surface-to-bulk diffusion is about 0.7 eV.[71] A higher barrier, 1.4 eV, has been found for diffusion on the surface. These barriers, in particular the second one, are larger than that required to diffuse an H atom from the Ru cluster to the oxide surface. In this case, the kinetic of the process would be dominated by H surface diffusion and not by metal/oxide interface diffusion. Further work is planned to specifically address this point and to extend the analysis also to ZrO_2.

From an electronic point of view, the addition of one H atom to TiO_2 or ZrO_2 leads to the reduction of the oxides with formation of localized Ti^{3+} $3d^1$ and Zr^{3+} $4d^1$ centers. We have been able to find localized solutions for these systems. In the presence of a deposited metal particle, the tendency to localize the charge on a single transition metal atom is more pronounced for TiO_2 than for ZrO_2 surfaces. This, however, is a delicate issue where the results clearly depend on the DFT +U approach (using a hybrid functional approach or a larger U parameter could produce slightly different results). However, the occurrence of a chemical reduction of the oxide by hydrogen addition by hydrogen spillover is clearly shown by the net atomic charges. In particular, when an H atom migrates from the Ru_{10} particle to the TiO_2 or ZrO_2 surfaces, the nuclear motion is accompanied by an electronic redistribution which

DOI: 10.1021/acscatal.5b01093
ACS Catal. 2015, 5, 5486−5495

results in charge flow from the metal to the oxide. Other potential reduction mechanisms, like the reaction of hydrogen with surface oxygen to form water that desorbs leaving behind an oxygen vacancy, does not seem to be competitive with the hydrogen spillover mechanism.

These theoretical results shed light on the atomistic mechanism of hydrogen spillover and are fully consistent with experimental observations. For instance, in a study of hydrogen spillover over Au/TiO_2, Panayotov and Yates[83] demonstrated that the rate of the spillover process is proportional to $P_{H_2}^{1/2}$, indicating that the mobile H atoms originate from the equilibrium dissociative adsorption of adsorbed H_2 on the Au particle (the main difference is that a barrier of 0.5 eV has been found for H_2 dissociation on the supported Au particles, while the reaction is barrierless on Ru_{10}). In the experiment, the diffusion of H atoms into the oxide is accompanied by the formation of trapped electrons in shallow trap states near the bottom of the conduction band edge. All these features are in line with the computational results presented in this study, which provides therefore a microscopic view of this complex phenomenon.

■ ASSOCIATED CONTENT

Supporting Information

The Supporting Information is available free of charge on the ACS Publications website at DOI: 10.1021/acscatal.5b01093.

Further analysis on the dissociation of H_2 at high loading and coordinates of a few representative structures (PDF)

■ AUTHOR INFORMATION

Corresponding Author

*Tel.: +39-2-64485219. E-mail: gianfranco.pacchioni@unimib.it.

Notes

The authors declare no competing financial interest.

■ ACKNOWLEDGMENTS

This work has been supported by the European Community's Seventh Framework Programme FP7/2007-2013 under Grant Agreement no. 604307 (CASCATBEL) and by Italian MIUR through the FIRB Project RBAP115AYN "Oxides at the nanoscale: multifunctionality and applications." The support of the COST Action CM1104 "Reducible oxide chemistry, structure and functions" is also gratefully acknowledged.

■ REFERENCES

(1) Pacchioni, G. *Phys. Chem. Chem. Phys.* **2013**, *15*, 1737−1757.
(2) Libuda, J.; Freund, H.- J. *Surf. Sci. Rep.* **2005**, *57*, 157−298.
(3) Somorjai, G. A.; Park, J. Y. *Chem. Soc. Rev.* **2008**, *37*, 2155−2162.
(4) Bell, A. T. *Science* **2003**, *299*, 1688−1691.
(5) Barteau, M. A. *Chem. Rev.* **1996**, *96*, 1413−1430.
(6) Pham, T. N.; Sooknoi, T.; Crossley, S. P.; Resasco, D. E. *ACS Catal.* **2013**, *3*, 2456−2473.
(7) Rajadurai, S. *Catal. Rev.: Sci. Eng.* **1994**, *36*, 385−403.
(8) Pacchioni, G. *ACS Catal.* **2014**, *4*, 2874−2888.
(9) Pham, T. N.; Shi, D. C.; Resasco, D. E. *Top. Catal.* **2014**, *57*, 706−714.
(10) Pham, T. N.; Shi, D. C.; Resasco, D. E. *J. Catal.* **2014**, *314*, 149−158.
(11) Chen, H.-Y. T; Tosoni, S.; Pacchioni, G. *J. Phys. Chem. C* **2015**, *119*, 10856−10868.
(12) Tosoni, S.; Chen, H.-Y. T; Pacchioni, G. *Surf. Sci.* **2015**, DOI: 10.1016/j.susc.2015.04.004.
(13) Sermon, P. A.; Bond, G. C. *Catal. Rev.: Sci. Eng.* **1974**, *8*, 211−239.
(14) McTaggart, F. K. *Nature* **1961**, *191*, 1192.
(15) Hoang, D. L.; Lieske, H. *Catal. Lett.* **1994**, *27*, 33−42.
(16) Rozanov, V. V.; Krylov, O. V. *Russ. Chem. Rev.* **1997**, *66*, 107−119.
(17) Prins, R. *Chem. Rev.* **2012**, *112*, 2714−2738.
(18) Khoobiar, S. *J. Phys. Chem.* **1964**, *68*, 411.
(19) Cucinotta, C. S.; Bernasconi, M.; Parrinello, M. *Phys. Rev. Lett.* **2011**, *107*, 206103.
(20) Dall'Agnol, C.; Gervasini, A.; Morazzoni, F.; Pinna, F.; Strukul, G.; Zanderighi, L. *J. Catal.* **1985**, *96*, 106−114.
(21) Fisher, I. A.; Bell, A. T. *J. Catal.* **1997**, *172*, 222−237.
(22) Zhu, Y.; Liu, D.; Meng, M. *Chem. Commun.* **2014**, *50*, 6049−6051.
(23) Panayotov, D. A.; Yates, J. T., Jr. *J. Phys. Chem. C* **2007**, *111*, 2959−2964.
(24) Panayotov, D. A.; Burrows, S. P.; Yates, J. T., Jr.; Morris, J. R. *J. Phys. Chem. C* **2011**, *115*, 22400−22408.
(25) Faccin, F.; Guedes, F. F.; Benvenutti, E. V.; Moro, C. C. *Ecletica Quim.* **2002**, *27*, 93−102.
(26) Vayssilov, G. N.; Gates, B. C.; Rösch, N. *Angew. Chem., Int. Ed.* **2003**, *42*, 1391−1394.
(27) Ivanova Shor, E. A.; Nasluzov, V. A.; Shor, A. M.; Vayssilov, G. N.; Rösch, N. *J. Phys. Chem. C* **2007**, *111*, 12340−12351.
(28) Hu, C. H.; Chizallet, C.; Mager-Maury, C.; Corral-Valero, M.; Sautet, P.; Toulhoat, H.; Raybaud, P. *J. Catal.* **2010**, *274*, 99−110.
(29) Mager-Maury, C.; Chizallet, C.; Sautet, P.; Raybaud, P. *ACS Catal.* **2012**, *2*, 1346−1357.
(30) Santana, J. A.; Rösch, N. *Phys. Chem. Chem. Phys.* **2012**, *14*, 16062−16069.
(31) Keren, E.; Soffer, A. *J. Catal.* **1977**, *50*, 43−55.
(32) Kresse, G.; Furthmüller, J. *Comput. Mater. Sci.* **1996**, *6*, 15−50.
(33) Blöchl, P. E. *Phys. Rev. B: Condens. Matter Mater. Phys.* **1994**, *50*, 17953−17979.
(34) Kresse, G.; Joubert, J. *Phys. Rev. B: Condens. Matter Mater. Phys.* **1999**, *59*, 1758−1775.
(35) Perdew, J. P.; Burke, K.; Ernzerhof, M. *Phys. Rev. Lett.* **1996**, *77*, 3865−3868.
(36) Anisimov, V. I.; Zaanen, J.; Andersen, O. K. *Phys. Rev. B: Condens. Matter Mater. Phys.* **1991**, *44*, 943−954.
(37) Dudarev, S. L.; Botton, G. A.; Savrasov, S. Y.; Humphreys, C. J.; Sutton, A. P. *Phys. Rev. B: Condens. Matter Mater. Phys.* **1998**, *57*, 1505−1509.
(38) Dagotto, E. *Rev. Mod. Phys.* **1994**, *66*, 763−840.
(39) Moreira, I. d. P. R.; Illas, F.; Martin, R. L. *Phys. Rev. B: Condens. Matter Mater. Phys.* **2002**, *65*, 155102.
(40) Rivero, P.; Moreira, I. de P. R.; Illas, F. *Phys. Rev. B: Condens. Matter Mater. Phys.* **2010**, *81*, 205123.
(41) Tosoni, S.; Lamiel-Garcia, O.; Fernandez Hevia, D.; Doña, J. M.; Illas, F. *J. Phys. Chem. C* **2012**, *116*, 12738−12746.
(42) Ortega, Y.; Lamiel-Garcia, O.; Hevia, D. F.; Tosoni, S.; Oviedo, J.; San-Miguel, M. A.; Illas, F. *Surf. Sci.* **2013**, *618*, 154−158.
(43) Syzgantseva, O. A.; Calatayud, M.; Minot, C. *J. Phys. Chem. C* **2012**, *116*, 6636−6644.
(44) Ghosh, T. B.; Dhabal, S.; Datta, A. K. *J. Appl. Phys.* **2003**, *94*, 4577−4582.
(45) Smith, S. J.; Stevens, R.; Liu, S. F.; Li, G. S.; Navrotsky, A.; Boerio-Goates, J.; Woodfield, B. F. *Am. Mineral.* **2009**, *94*, 236−243.
(46) Hanaor, D. A. H.; Sorrell, C. C. *J. Mater. Sci.* **2011**, *46*, 855−874.
(47) Augustynski, J. *Electrochim. Acta* **1993**, *38*, 43−46.
(48) Linsebigler, A. L.; Lu, G. Q.; Yates, J. T., Jr. *Chem. Rev.* **1995**, *95*, 735−758.
(49) Hadjiivanov, K. I.; Klissurski, D. G. *Chem. Soc. Rev.* **1996**, *25*, 61−69.
(50) Kavan, L.; Grätzel, M.; Gilbert, S. E.; Klemenz, C.; Scheel, H. J. *J. Am. Chem. Soc.* **1996**, *118*, 6716−6723.
(51) Diebold, U.; Ruzycki, N.; Herman, G. S.; Selloni, A. *Catal. Today* **2003**, *85*, 93−100.

DOI: 10.1021/acscatal.5b01093
ACS Catal. 2015, 5, 5486−5495

(52) Leger, J. M.; Tomaszewski, P. E.; Atouf, A.; Pereira, A. S. *Phys. Rev. B: Condens. Matter Mater. Phys.* **1993**, *47*, 14075−14083.
(53) Kisi, E. H.; Howard, C. J. *Key Eng. Mater.* **1998**, *153*−*154*, 1−39.
(54) Dash, L. K.; Vast, N.; Baranek, P.; Cheynet, M. C.; Reining, L. *Phys. Rev. B: Condens. Matter Mater. Phys.* **2004**, *70*, 245116.
(55) Shukla, S.; Seal, S. *Int. Mater. Rev.* **2005**, *50*, 45−64.
(56) Hofmann, A.; Clark, S. J.; Oppel, M.; Hahndorf, I. *Phys. Chem. Chem. Phys.* **2002**, *4*, 3500−3508.
(57) Christensen, A.; Carter, E. A. *Phys. Rev. B: Condens. Matter Mater. Phys.* **1998**, *58*, 8050−8064.
(58) Haase, F.; Sauer, J. *J. Am. Chem. Soc.* **1998**, *120*, 13503−13512.
(59) Eichler, A.; Kresse, G. *Phys. Rev. B: Condens. Matter Mater. Phys.* **2004**, *69*, 045402.
(60) Ganduglia-Pirovano, M. V.; Hofmann, A.; Sauer, J. *Surf. Sci. Rep.* **2007**, *62*, 219−270.
(61) Bader, R. F. W. *Chem. Rev.* **1991**, *91*, 893−928.
(62) Stone, F. S.; Garrone, E.; Zecchina, A. *Mater. Chem. Phys.* **1985**, *13*, 331−346.
(63) Chen, H.-Y. T.; Giordano, L.; Pacchioni, G. *J. Phys. Chem. C* **2013**, *117*, 10623−10629.
(64) Leconte, A.; Markovits, M.; Skalli, M. K.; Minot, C.; Belmajdoub, A. *Surf. Sci.* **2002**, *497*, 194−204.
(65) Calatayud, M.; Markovits, A.; Minot, C. *Catal. Today* **2004**, *89*, 269−278.
(66) Panayotov, D. A.; Yates, J. T., Jr. *Chem. Phys. Lett.* **2007**, *436*, 204−208.
(67) Peacock, P. W.; Robertson, J. *Appl. Phys. Lett.* **2003**, *83*, 2025.
(68) Di Valentin, C.; Pacchioni, G.; Selloni, A. *Phys. Rev. Lett.* **2006**, *97*, 166803.
(69) Koudriachova, M. V.; De Leeuw, S. W.; Harrison, N. M. *Phys. Rev. B: Condens. Matter Mater. Phys.* **2004**, *70*, 165421.
(70) Aschauer, U.; Selloni, A. *Phys. Chem. Chem. Phys.* **2012**, *14*, 16595−16602.
(71) Islam, M. M.; Calatayud, M.; Pacchioni, G. *J. Phys. Chem. C* **2011**, *115*, 6809−6814.
(72) Di Valentin, C.; Pacchioni, G.; Selloni, A. *J. Phys. Chem. C* **2009**, *113*, 20543−20552.
(73) Deskins, N. A.; Dupuis, M. *Phys. Rev. B: Condens. Matter Mater. Phys.* **2007**, *75*, 195212.
(74) Finazzi, E.; Di Valentin, C.; Pacchioni, G.; Selloni, A. *J. Chem. Phys.* **2008**, *129*, 154113.
(75) Hofmann, A.; Clark, S. J.; Oppel, M.; Hahndorf, I. *Phys. Chem. Chem. Phys.* **2002**, *4*, 3500−3508.
(76) Chen, L.; Cooper, A. C.; Pez, G. P.; Cheng, H. *J. Phys. Chem. C* **2007**, *111*, 5514−5519.
(77) Singh, A. K.; Ribas, M. A.; Yakobson, B. I. *ACS Nano* **2009**, *3*, 1657−1662.
(78) Mager-Maury, C.; Bonnard, G.; Chizallet, C.; Sautet, P.; Raybaud, P. *ChemCatChem* **2011**, *3*, 200−207.
(79) Gorczyca, A.; Moizan, V.; Chizallet, C.; Proux, O.; Del Net, W.; Lahera, E.; Hazemann, J.-L.; Raybaud, P.; Joly, Y. *Angew. Chem., Int. Ed.* **2014**, *53*, 12426−12429.
(80) Henkelman, G.; Jónsson, H.; Uberuaga, B. P. *J. Chem. Phys.* **2000**, *113*, 9901−9904.
(81) Arrouvel, C.; Digne, M.; Breysse, M.; Toulhoat, H.; Raybaud, P. *J. Catal.* **2004**, *222*, 152−166.
(82) Añez, R.; Sierraalta, A.; Martorell, G.; Sautet, P. *Surf. Sci.* **2009**, *603*, 2526−2531.
(83) Panayotov, D. A.; Yates, J. T., Jr. *J. Phys. Chem. C* **2007**, *111*, 2959−2964.

DOI: 10.1021/acscatal.5b01093
ACS Catal. 2015, 5, 5486−5495